

Novel Series of Diaminoanthraquinone-Based  $\pi$ -Extendable Building Blocks with Tunable Optoelectronic PropertiesGanesh Masilamani,<sup>◆</sup> Harikrishna Batchu,<sup>◆</sup> Dana Amsallem, and Anjan Bedi<sup>\*</sup>Cite This: *ACS Omega* 2022, 7, 25874–25880

Read Online

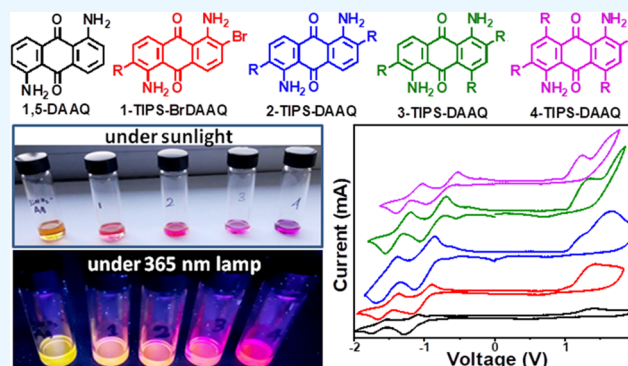
ACCESS |

Metrics &amp; More

Article Recommendations

Supporting Information

**ABSTRACT:** We have achieved the first series of DAAQ-based building blocks, viz., *n*-TIPS-DAAQs (*n* = 1–4), and unraveled a rational design of their  $\pi$ -extension. Sequentially increasing numbers (*n*) of the exocyclic  $\pi$ -linkers showed (a) a systematic bathochromic shift in both absorption and emission spectra, (b) selective stabilization of the lowest-unoccupied molecular orbital (LUMO), and (c) unselective changes in the  $S_0/S_1$  states. To our surprise, the LUMO level of 4-TIPS-DAAQ (−3.72 eV) was found to be comparable to that of PC<sub>60</sub>BM.



## 1. INTRODUCTION

Among the common organic dyes and pigments, diaminoanthraquinones (DAAQs) (Figure 1) have grabbed attention as

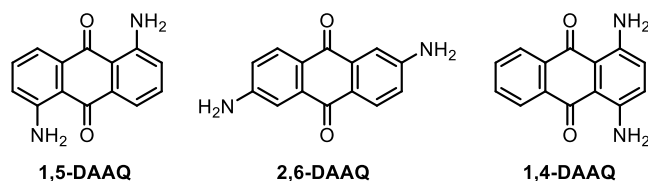


Figure 1. Isomers of DAAQs.

these have attractive photophysical properties and potential toward applications in multiple important directions.<sup>1</sup> In recent years, DAAQs have developed from the common organic dyestuffs to coloring superhydrophobic cotton.<sup>2</sup> On the other hand, N-substituted DAAQs are applied in LCD panels,<sup>3</sup> nonlinear optics,<sup>4</sup> etc., which renders them important materials for high-speed optical communication networks, storage of information, optical switches, optical limiting devices, nano-devices, etc. The reversible redox behavior of the DAAQs makes them a suitable candidate in redox-flow batteries,<sup>5</sup> energy conversion devices,<sup>6</sup> and electro-swing carbon capture devices.<sup>7</sup> Recently, Yao et al. showed that 1,5-DAAQ carries potential as a material for advancement in nanoscale optical devices, networks, and circuits.<sup>8</sup> Despite the promising developments in these area, DAAQs with an insightful work on the structure–property relationship in such systems are scarce or limited to only N-substitutions.<sup>9</sup> This hinders their potential applications in relevant fields. One approach to further exploration of DAAQs could be inserting

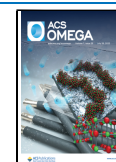
$\pi$ -extendable anchoring group(s) on the anthraquinone part of DAAQs to achieve elongated  $\pi$ -systems. But extension of DAAQ via common electrophilic substitution reactions or C–H activation is not known in the DAAQ family, which may be because of an outstanding synthetic challenge.

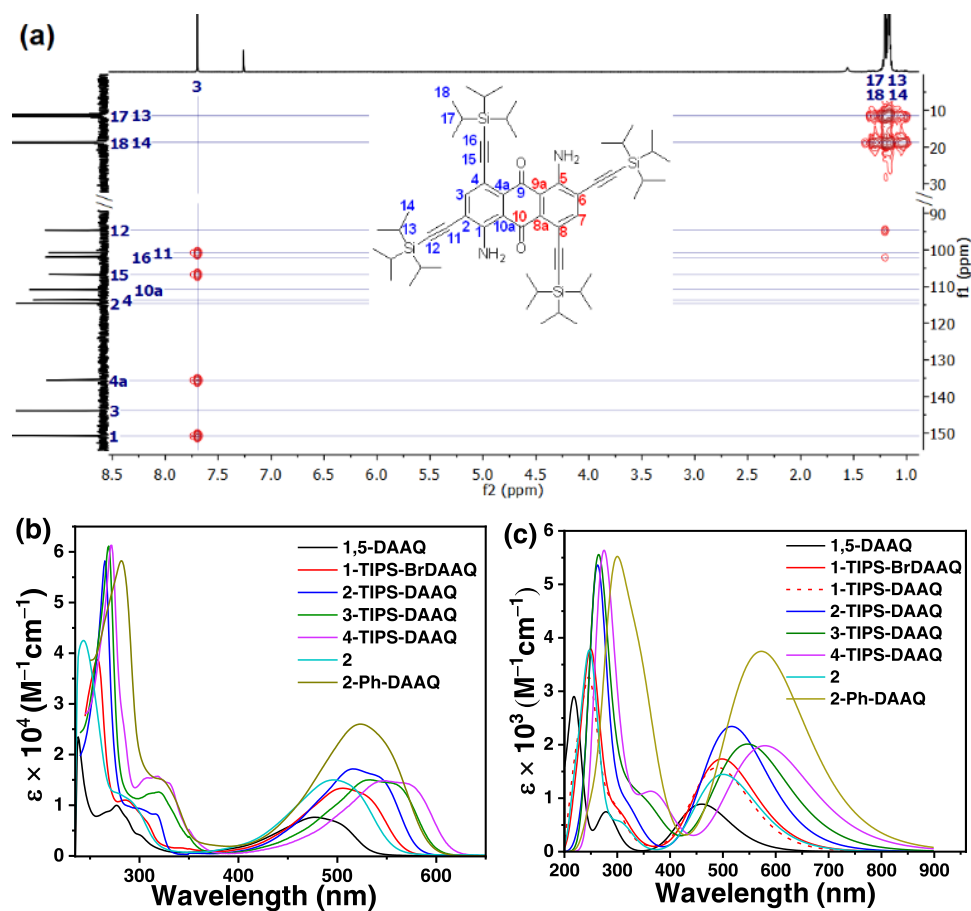
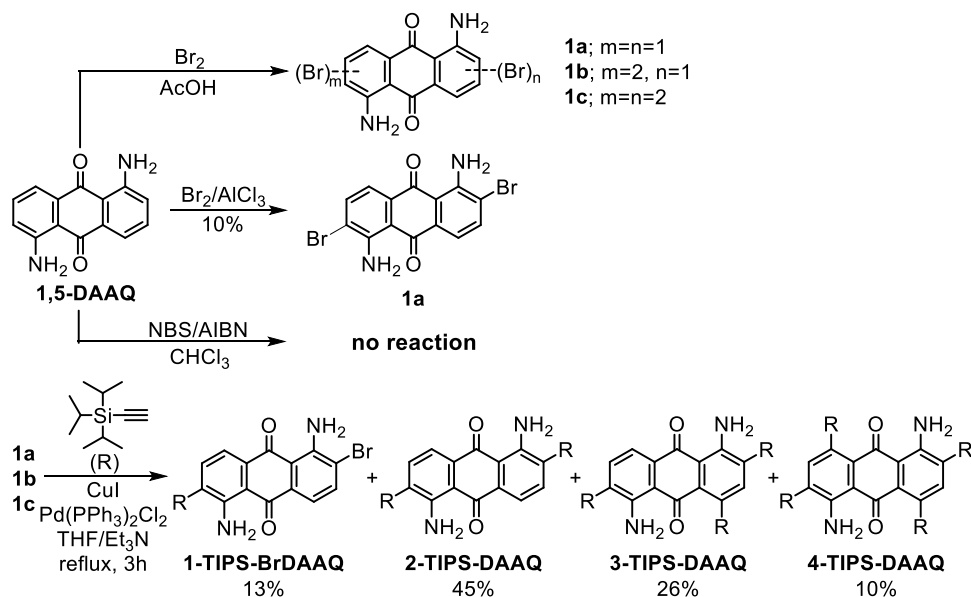
On the other hand, the attractive optoelectronic properties of DAAQs are known to be dominated by a  $\pi \rightarrow \pi^*$  transition.<sup>10</sup> In particular, in polar solvents, DAAQ remains in a dipolar form. As a result, various substitutions on the  $-\text{NH}_2$  groups can tune intramolecular charge transfer (ICT) to different extents. But there exists no avenue to functionalize the DAAQ dyes through any other position than the major functional groups that build up the elegant chromophore. So, any structure–property relationship between substitutions on the anthraquinone core of the DAAQ and promising improvements in optoelectronic properties is unknown. This may be because of the lack of synthetic methods to substitute the relatively inactive benzene rings in DAAQs toward electrophilic substitutions. To achieve the DAAQ core in multiple directions for  $\pi$ -extension and study the effect of sequentially increasing number of identical substitutions on optoelectronic properties, focus should be given not to anticipate any steric factor due to the substitutions, which could distort the planarity and impart additional electronic

Received: June 9, 2022

Accepted: June 28, 2022

Published: July 13, 2022

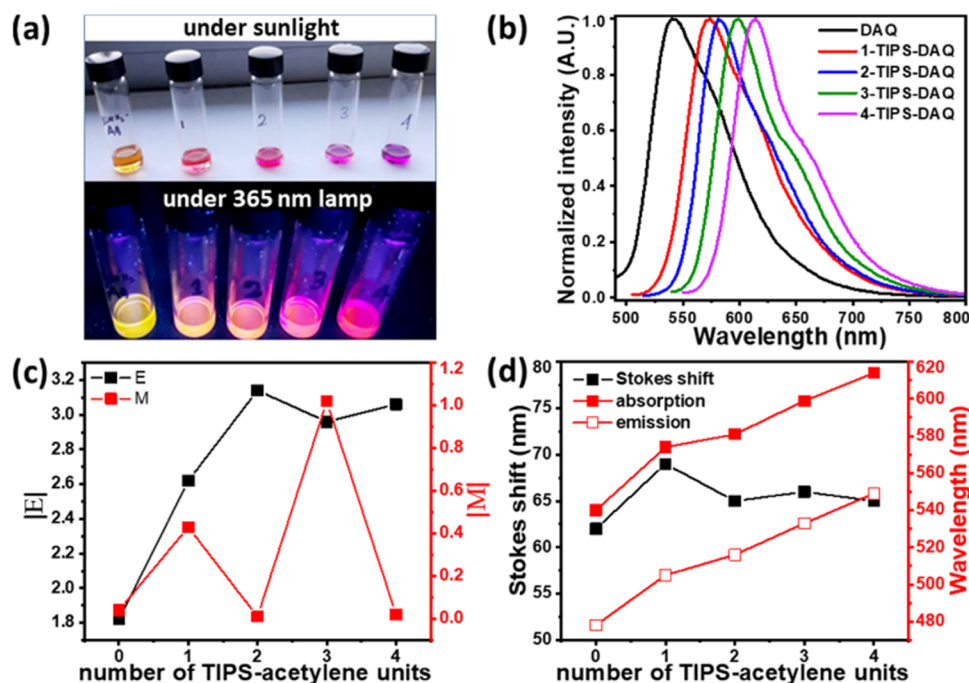
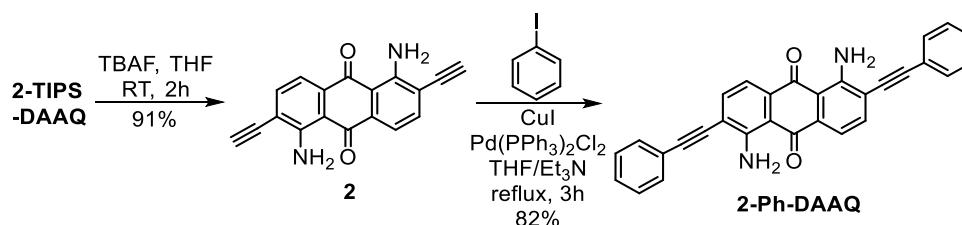


Scheme 1. Synthesis of *n*-TIPS-DAAQs

**Figure 2.** (a) HMBC NMR spectra (relevant part) of 4-TIPS-DAAQ recorded at 298 K in  $\text{CDCl}_3$ ; (b) experimental UV-vis spectra in chloroform; and (c) computationally (TDDFT-B3LYP-6-31G(d)) obtained gas-phase UV-vis spectra of the DAAQs.

effects. Another feature that leads to interesting optoelectronic properties is the intramolecular hydrogen bonding in 1,5-DAAQ, unlike in 2,6-DAAQ.<sup>9</sup> Additionally, the aromatic ring current in either sides of the central quinone ring in 1,4-DAAQ is not of uniform in nature unlike in 1,5-DAAQ. This could hinder in achieving a building block with symmetrically

delocalized  $\pi$ -electrons. Considering these, we chose to functionalize 1,5-DAAQ over its any other isomers. Contextually, we recently reported a novel method to selectively brominate the 2- and 6-positions of 1,5-DAAQ.<sup>11</sup> Inspired by that, we attempted to address the aforementioned problems by systematically increasing the number of identical substitutions

Scheme 2. Synthesis of **2** and  $\pi$ -extended derivative **2-Ph-DAAQ**

**Figure 3.** (a) Appearance of the DAAQs in the chloroform solution under different light sources; (b) emission spectra; (c) calculated (TDDFT-B3LYP-6-31G(d)) transition dipole moments (TDMs); and (d) Stokes shift in chloroform. In (c) and (d) X-axes, 0 = 1,5-DAAQ, 1 = 1-TIPS-BrDAAQ, 2 = 2-TIPS-DAAQ, 3 = 3-TIPS-DAAQ, and 4 = 4-TIPS-DAAQ.  $|E|$  = transition electric dipole moment.  $|M|$  = transition magnetic dipole moment.

on 1,5-DAAQ without affecting the existing functional groups and the planarity of the 1,5-DAAQ core.

## 2. RESULTS AND DISCUSSION

Our initial attempts to brominate 1,5-DAAQ such as (i)  $AlCl_3$ -mediated bromination or (ii) use of the NBS/AIBN mixture as a brominating agent resulted in very low or no conversion to doubly brominated products **1a**, respectively (Scheme 1). So, perbromination was performed by adding elemental bromine (2.5 equiv) to 1,5-DAAQ in glacial acetic acid at room temperature. The resulting crude mixture of bromo-DAAQs (**1a–c**) underwent the Sonogashira coupling with tri(isopropyl)silyl (TIPS) acetylene (3 equiv) in the presence of copper(I) iodide and bis(triphenylphosphine)-palladium(II) dichloride ( $Pd(PPh_3)_2Cl_2$ ) to result in  $n$ -TIPS-DAAQs ( $n = 1–4$ ) within a single step. The TIPS-acetylene groups provide outstanding solubility toward studying optoelectronic properties in common organic solvents.

The perbrominated DAAQs were insoluble in common organic solvents, which limited us to isolate and characterize the mixture of **1a–c**. So, the lingering question of regioselectivity for such bromination in the presence of two functional groups, i.e.,  $>C=O$  and  $-NH_2$  in 1,5-DAAQ, was unanswered. However, we could isolate the  $n$ -TIPS-DAAQs

on a silica column using hexane/dichloromethane as an eluent and characterize them by  $^1H$ ,  $^{13}C$  NMR, and HRMS. Previously, we reported 2-TIPS-DAAQ with unambiguous structural characterization.<sup>11</sup> So, to confirm the structure of 3/4-TIPS-DAAQs, an adequate method was used to perform 2D correlation spectroscopy (COSY, HSQC, and HMBC) only for 4-TIPS-DAAQ (Figures S10–S12). No signal in COSY and the presence of one signal in the aromatic region in HSQC spectra confirmed an isolated secondary carbon atom (C3). Most importantly, HMBC showed four signals correlating  $^1H$ -C(3) with the C1, C4a, C11, and C15, among which two originated from correlation of the C-atom of the  $-C\equiv C-$  bond and the aromatic H-atom (Figure 2a). This confirms the aforementioned structure of 4-TIPS-DAAQ (Scheme 1) and the regioselectivity of the bromination reaction at 2-, 4-, 6-, and 8-positions of 1,5-DAAQ.<sup>12</sup>

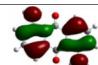
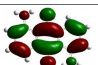
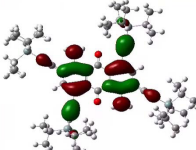
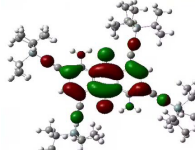
To explore  $n$ -TIPS-DAAQs as potential building blocks, a rational approach was demonstrated (Scheme 2). The TIPS groups of 2-TIPS-DAAQ were removed using tetra-*n*-butylammonium fluoride with 91% yield of **2**. The solubility of **2** was comparatively better than the perbrominated mixture **1a–c**. Despite that,  $^{13}C$  NMR spectra in THF- $d_6$  were reliably recorded. The Sonogashira coupling was achieved with **2**, iodobenzene, and  $Pd(PPh_3)_2Cl_2$  in triethyl-

amine/THF (1/1) as a solvent under mild temperature conditions. Thus, the undisturbed  $-\text{NH}_2$  groups in *n*-TIPS-DAAQ, **2**, and 2-Ph-DAAQ leave open further options to extend the core through either base or Cu(II) catalyzed C–N bond formation<sup>13</sup> under mild conditions. We anticipate that Scheme 2 will be suitable for all *n*-TIPS-DAAQs. Therefore, this current design of  $\pi$ -extendable 1,5-DAAQ-based building blocks could be flexible from both  $-\text{C}\equiv\text{C}-$  and  $-\text{NH}_2$  sites for making longer  $\pi$ -conjugated systems, which was never achieved so far, until this report. We anticipate that such chemistry could be applied to several other systems of significant interest with similar synthetic difficulties. In a similar context of achieving synthetically challenging novel building blocks, the selective bromination of perylene diimide under simple conditions by Rybtchinski et al.<sup>14</sup> can be referred, which triggered the path to larger systems for superior organic electronic materials.

The UV–vis spectra of the DAAQs displayed three major transitions around 250, 270–350, and 360–620 nm (Figure 2b). The longest wavelength band can be ascribed to the  $\pi \rightarrow \pi^*$  transition contributed mostly by the HOMO  $\rightarrow$  LUMO transition (Table S4). Appearance of the *n*-TIPS-DAAQs in the solution varied from brick-red to purple (Figure 3a), which was manifested by the systematic bathochromic shift in the UV–vis spectra upon a sequential increase in the number of TIPS-acetylenes (Table S1). This could be attributed to a continuous decrease in the HOMO–LUMO gap (HLG) due to extended  $\pi$ -delocalization. This band was associated with a noticeable vibronic shoulder. Polar solvents perturb the electronic states of such molecules possessing permanent dipole moment.<sup>15</sup> So, to estimate the changes in the HLG against the increasing number of the acetylene units, we used the same solvent chloroform (a good solvent that avoids self-aggregation of *n*-TIPS-DAAQs) for photophysical studies. We did not observe substantial changes in the full-width-at-half-maxima (FWHM) with increasing chromophore length, but the vibronic shoulder appeared noticeably at a distance of 0.06 eV from the peak for 3-TIPS-DAAQ and 4-TIPS-DAAQ. Remarkably, extending the building block **2** to two additional phenyl rings on either sides of it in 2-Ph-DAAQ red-shifted the  $\pi \rightarrow \pi^*$  transition by 23 nm while it showed 1.7 times magnification of the molar extinction coefficient ( $\epsilon = 26\,011\text{ M}^{-1}\text{ cm}^{-1}$ ). This renders the preference to the latter to be used as the active material in dye-sensitized solar cells ( $\epsilon > 26\,000\text{ M}^{-1}\text{ cm}^{-1}$  in the visible range) compared to the rest of the dyes here.

Computationally obtained (TDDFT-B3LYP-6-31G(d)) spectra complemented the peaks and trends of bathochromic shifts quite efficiently (Figure 2c). Any overall trend in the  $\epsilon$  against the increase in *n* was not observed experimentally for the *n*-TIPS-DAAQs, which was also supported by calculations (Figure S17). The oscillator strength (*f*) was found to be higher in all of the *n*-TIPS-DAAQs compared to 1,5-DAAQ. This enhancement in *f* of the  $\pi \rightarrow \pi^*$  transition is because of an increase in the magnitude of the transition electric dipole moment ( $|E|$ ) upon insertion of the acetylenes (Figures 3c and S19 and Table S5). The highest value of  $\epsilon$  for the  $\pi \rightarrow \pi^*$  transition signifies an end-to-end  $\pi$ -conjugation in 2-TIPS-DAAQ. Notably, in 3-TIPS-DAAQ and 4-TIPS-DAAQ, a relatively higher electron density in the acetylene units attached on either 4- or 8-positions of the 1,5-DAAQ core was observed, compared to that on other acetylenes attached to 2- and 6-positions (Tables 1 and S6). However, uniform

**Table 1.** Frontier Molecular Orbitals (FMOs) of 1,5-DAAQ and 4-TIPS-DAAQ

	HOMO	LUMO
1,5-DAAQ		
4-TIPS-DAAQ		

delocalization of the electron density in all paths of conjugation was observed in their LUMO levels. A subtle decline in  $\epsilon$  with systematically increasing *n* beyond 2-TIPS-DAAQ is due to an anomaly in the dipole strength (DS). The DS was controlled by a stronger  $|E|$ . Contextually, the more symmetric 2-TIPS-DAAQ and 4-TIPS-DAAQ possessed the transition magnetic dipole moment  $|M|$  as low as that of 1,5-DAAQ (nearly zero) (Figure 3c). In comparison, less symmetric 1-TIPS-BrDAAQ, 3-TIPS-DAAQ, and hypothetical 1-TIPS-DAAQ garnered significant magnitudes of  $|M|$ . Thus, DS increased from 1,5-DAAQ to 2-TIPS-DAAQ and then kept on decreasing afterward. So, *f* varies in the same way which reflects in the variation pattern of  $\epsilon$  as well. Remarkably, the 1.7 times increase in  $\epsilon$  for 2-Ph-DAAQ compared to **2** in experimental spectra could be explained by the 1.5 times increase in  $|E|$  by elongated end-to-end transition dipole compared to that of **2**.

Only 4-TIPS-DAAQ displayed a distinctly separable electronic transition within 270–350 nm in the computationally obtained spectra. UV–vis spectra from the polarizable continuum model (PCM) calculation (Figure S17) using chloroform as a solvent could not provide any additional insights. This band is comparable to the 270–350 nm band in the experimentally obtained spectra with weak optical density. It was constructed of several transitions to a LUMO level from HOMO-*n* levels (*n* = 1, 2, etc.) in different *n*-TIPS-DAAQs. On the other hand, the brightest peak in the UV–vis spectra is mostly due to transition to a LUMO + 1 level from HOMO-*n* levels (*n* = 1, 2, etc.). This band, constructed of several states of similar oscillator strengths and contributed by nonrecurring MOs in different *n*-TIPS-DAAQs, limits any further discussion. Upon excitation of the DAAQs at their  $\lambda_{\text{max}}(\pi \rightarrow \pi^*)$ , yellow to pink emission was observed (Figure 3a). Emission spectra (Figure 3b) displayed a bathochromic shift upon increasing the number of  $\pi$ -linkers identically to their absorption spectra (Table S1). Notably, the Stokes shift (Figure 3d) and the number of vibronic structures remained similar in all *n*-TIPS-DAAQs, which hints to the fact that the  $\pi$ -extension does not preferably affect the properties of either of the  $S_0$  or  $S_1$  states significantly. The vibronic shoulder became prominent in the oversubstituted *n*-TIPS-DAAQs (*n* > 2). The negligibly low quantum yields within the instrumental error ranges limited us to build up further correlation.

*n*-TIPS-DAAQs displayed multiple redox phenomena (Figure 4) in cyclic voltammetry (CV). Specially, the elegant reversible cathodic reduction features of the DAAQ core in all the newly synthesized molecules favor the design principle of establishing 1,5-DAAQ-based building blocks. The HOMO levels calculated from the onset oxidation potential ( $E_{\text{onset}}^{\text{ox}}$ ) remained unaltered ( $\sim -5.3$  eV) even after multiple acetylene



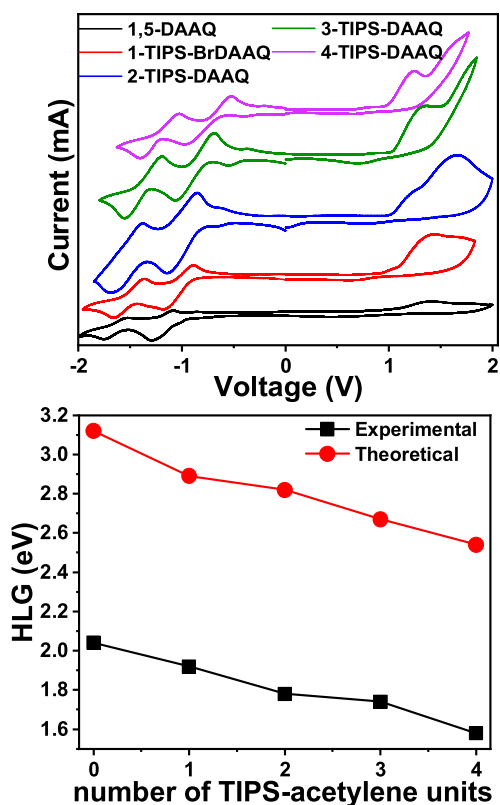


**Figure 4.** Top CV of 1,5-DAAQ and *n*-TIPS-DAAQs in dichloromethane. Down, comparison of the HOMO–LUMO gap (HLG) obtained from CV and DFT calculation (B3LYP-6-31G(d)); X-axis: 0 = 1,5-DAAQ, 1 = 1-TIPS-BrDAAQ, 2 = 2-TIPS-DAAQ, 3 = 3-TIPS-DAAQ, and 4 = 4-TIPS-DAAQ.

substitutions (Table S1). On the contrary, the LUMO levels calculated from onset reduction potential ( $E_{\text{onset}}^{\text{red}}$ ) became systematically stabilized. As a result, the HLG followed a decreasing trend upon sequential insertion of acetylenes into the DAAQ backbone. For example, the LUMO level was stabilized significantly by 0.44 eV from 1,5-DAAQ to 4-TIPS-DAAQ, which was reflected in the trend of change in the solution state optical HOMO–LUMO gap ( $E_{\text{g}}^{\text{opt}}$ ) (0.29 eV) between the two. DFT calculations (DFT-B3LYP-6-31G(d)) complemented this lowering of the HLG elegantly. With increasing *n* in *n*-TIPS-DAAQs, computationally obtained HOMO levels were uplifted by a small factor, while the LUMO levels were stabilized to a double extent. For example, from 1,5-DAAQ to 4-TIPS-DAAQ, the calculated (DFT-B3LYP-6-31G(d)) energy of the HOMO increased from  $-5.55$  to  $-5.37$  eV but the LUMO stabilized from  $-2.44$  to  $-2.83$  eV (Figure S18). Upon increasing *n* in *n*-TIPS-DAAQs, the quinoidal character is not expected to differ substantially as bond length alterations in the DAAQ core remained within 0.001 Å compared to that of 1,5-DAAQ. So, the lowering of the HLG is a manifestation of increasing scope and directions of  $\pi$ -delocalization pathways. The selective stabilization of the LUMO could be promising as it fulfills the criteria of lowering the bandgap in extended  $\pi$ -systems toward application in organic electronics. To our surprise, the LUMO (calculated from CV) of 4-TIPS-DAAQ ( $-3.72$  eV) is remarkably close to that of PC<sub>60</sub>BM ( $-3.70$  eV), which fulfills the energy-match criterion of an acceptor material in the recently evolving and promising research area of nonfullerene BHJ solar cells.<sup>16</sup>

### 3. CONCLUSIONS

In conclusion, we have successfully achieved a method to sequentially install increasing number of pathways to extend the elegant  $\pi$ -system 1,5-DAAQ without affecting the  $-\text{NH}_2$  and  $>\text{C}=\text{O}$  groups and its planarity (Table S2). In addition, extension of 2-TIPS-DAAQ toward a longer  $\pi$ -system 2-Ph-DAAQ was achieved quite efficiently with high yield. Very interestingly, the increasing number of acetylene substitutions offered: (a) visual color changes of the DAAQs due to differential absorption and emission, (b) selective stabilization of the LUMO between the FMOs, and (c) unselective changes in the properties of the  $S_0$  and  $S_1$  states. DFT computation complemented the trend observed in (a)  $\epsilon$ , (b) energy of the FMOs, and (c) the HLGs. Additionally, *n*-TIPS-DAAQs were found to be brighter in the UV–vis absorption spectra because of stronger TDMs than 1,5-DAAQ. Elongation of 2 to 2-Ph-DAAQ showed a bathochromic shift of 23 nm and 1.7 times of hyperchromic shift in the  $\pi \rightarrow \pi^*$  transition in UV–vis spectra. CV displayed the signature pattern of two reversible reductions in all *n*-TIPS-DAAQs. The selective stabilization of the LUMO promises to design new n-type organic electronic materials and low-bandgap materials. Notably, by sequentially increasing the number of TIPS-acetylenes on the 1,5-DAAQ core, we were able to achieve a LUMO energy of  $-3.72$  eV for 4-TIPS-DAAQ, which is comparable to that of PC<sub>60</sub>BM. In *n*-TIPS-DAAQs with attractive optoelectronic features, multiple pathways for  $\pi$ -extension could serve as important building blocks toward materials for future applications in areas such as organic electronics, dyes, optics, energy conversion devices. Some of these applications are currently in progress.

### 4. EXPERIMENTAL SECTION

Commercially available reagents and chemicals were used without further purification unless otherwise stated. Technical grade 1,5-DAAQ (85%) was purchased from Sigma-Aldrich. Column chromatography was performed using silica gel (100–200 mesh). <sup>1</sup>H and <sup>13</sup>C NMR spectra were recorded in the solution on Bruker AVIII 400 MHz and 500 MHz spectrometers using tetramethylsilane (TMS) as an external standard. The spectra were recorded using chloroform-*d* and tetrahydrofuran-*d*<sub>8</sub> as solvents. Chemical shifts are expressed in  $\delta$  (ppm) units. UV–vis absorption spectra were recorded using an Agilent Cary-5000 spectrophotometer. The spectra were measured using a quartz cuvette (1 cm) at 25 °C. The absorption wavelengths are reported in nm with the molar extinction coefficient  $\epsilon$  ( $\text{M}^{-1} \text{cm}^{-1}$ ) in brackets. Steady state fluorescence measurements were performed on a HORIBA JOBIN YVON Fluoromax-4 spectrofluorometer with the excitation/emission geometry at right angles. High-resolution mass spectra were measured on an HR Q-TOF LCMS and Waters Micromass GCT Premier Mass Spectrometer using ESI in a positive mode.

For electrochemical measurements, dichloromethane was used as a solvent containing 0.1 M tetra-*n*-butylammonium perchlorate (TBAPC) as an electrolyte. Ag/AgCl was used as a pseudo-reference electrode by dipping a silver wire in an aqueous solution of FeCl<sub>3</sub> and HCl. Platinum-disk and platinum-wire electrodes were applied as working and counter electrodes, respectively. All electrochemical measurements were performed under a dry nitrogen atmosphere. Anhydrous dichloromethane was purchased from Sigma-Aldrich and used as received. The half-wave oxidation potential for the

ferrocene/ferrocenium couple ( $E_{1/2}^{\text{Fc}/\text{Fc}^+}$ ) was externally measured to be 0.47 V under identical conditions used for other experiments.

**4.1. Synthesis of the Brominated 1,5-DAAQs (1a–c).**  
**4.1.1. Bromination Using Elemental Bromine and Aluminum(III) Chloride.** In a two-neck round-bottom (RB) flask were added aluminum(III) chloride (1.93 g, 14.44 mmol), **1,5-DAAQ** (85%, 1 g, 3.61 mmol), and bromine (0.74 mL, 14.44 mmol) under an inert atmosphere, and it was heated to 59 °C for 72 h. The reaction, monitored by  $^1\text{H}$  NMR spectra, did not show any progress further. The reaction mixture was taken to a chilled bath, quenched with ice. The resulting mixture was filtered through a Büchner funnel and washed with excess of water and dried to afford a reddish-brown solid **1a**<sup>17</sup> (143 mg, 10%).  $^1\text{H}$  NMR (400 MHz,  $\text{CDCl}_3$ )  $\delta$  (ppm) 7.80 (d,  $J = 8.0$  Hz, 2H), 7.51 (d,  $J = 8.0$  Hz, 2H).

**4.1.2. Bromination Using Elemental Bromine and Glacial Acetic Acid.** In a solution of **1,5-DAAQ** (85%, 1.00 g, 3.61 mmol) in glacial acetic acid (10 mL) was added a solution of elemental bromine (0.46 mL, 9.03 mmol) in glacial acetic acid (5 mL). The reaction mixture was kept under stirring for 6 h and then filtered through a Whatman 42 filter paper kept on a Büchner funnel under vacuum. The filtrate was washed sequentially with water (100 mL), 30% sodium bicarbonate solution (50 mL), and water (100 mL) to leave a dark brown solid. This crude solid was used for the next step without further purification.

**4.2. Synthesis of *n*-TIPS-DAAQs.** The aforementioned brown crude solid **1a–c** (1.77 g) was added to a thoroughly purged solution of THF (20 mL) and triethylamine (15 mL) kept in an oven-dried two-neck RB flask equipped with a magnetic stirrer and a condenser and purged thoroughly with nitrogen for 20 min. Triisopropylsilyl acetylene (2.02 mL, 9.03 mmol) and CuI (0.17 g, 0.90 mmol) were added to the mixture under a positive nitrogen flow followed by Pd( $\text{PPh}_3$ )<sub>2</sub>Cl<sub>2</sub> (0.32 g, 0.45 mmol). The mixture was then heated to reflux for 4 h. The solvent was removed in a rotavapor, and the resulting semi-solid mixture was subjected to silica gel chromatography using hexane to dichloromethane/hexane (3:17) to afford *n*-TIPS-DAAQs. Overall isolated yields of two steps are reported here.

**4.2.1. 1-TIPS-BrDAAQ.** Brownish-red solid (224 mg, 13%).  $^1\text{H}$  NMR (400 MHz,  $\text{CDCl}_3$ )  $\delta$  (ppm) 7.77 (d,  $J = 8.1$  Hz, 2H), 7.64 (d,  $J = 8.1$  Hz, 2H), 7.55 (d,  $J = 8.1$  Hz, 2H), 7.49 (d,  $J = 8.1$  Hz, 2H), 1.16 (d,  $J = 3.8$  Hz, 21H).  $^{13}\text{C}$  NMR (126 MHz,  $\text{CDCl}_3$ )  $\delta$  (ppm) 184.6, 151.4, 147.6, 137.8, 137.6, 134.88, 134.85, 116.7, 116.5, 115.6, 115.3, 114.4, 112.9, 102.0, 101.7, 18.7, 11.2. HR-ESI-MS  $m/z$  (%): calcd for  $\text{C}_{25}\text{H}_{30}\text{BrN}_2\text{O}_2\text{Si}^+$  ( $[\text{M} + \text{H}]^+$ ), 497.1260; found 497.1283. UV-vis ( $\text{CHCl}_3$ ):  $\lambda_{\text{max}}$  ( $\epsilon$ ) = 258(38 775), 285(11 012), 505 nm ( $13\ 345\ \text{M}^{-1}\ \text{cm}^{-1}$ ).

**4.2.2. 2-TIPS-DAAQ.** Dark red solid (958 mg, 45%).  $^1\text{H}$  NMR (400 MHz,  $\text{CDCl}_3$ )  $\delta$  (ppm) 7.63 (d,  $J = 7.8$  Hz, 2H), 7.55 (d,  $J = 7.8$  Hz, 2H), 1.16 (br, 42H).  $^{13}\text{C}$  NMR (126 MHz,  $\text{CDCl}_3$ )  $\delta$  (ppm) 184.9, 151.4, 137.5, 135.1, 115.4, 115.0, 113.2, 101.8, 101.8, 18.7, 11.2. HR-ESI-MS  $m/z$  (%): calcd for  $\text{C}_{36}\text{H}_{51}\text{N}_2\text{O}_2\text{Si}_2^+$  ( $[\text{M} + \text{H}]^+$ ), 599.3474; found 599.3489. UV-vis ( $\text{CHCl}_3$ ):  $\lambda_{\text{max}}$  ( $\epsilon$ ) = 265(59 229), 297(10 522), 315(9279), 517 nm ( $17\ 169\ \text{M}^{-1}\ \text{cm}^{-1}$ ).

**4.2.3. 3-TIPS-DAAQ.** Dark pink solid (639 mg, 26%).  $^1\text{H}$  NMR (400 MHz,  $\text{CDCl}_3$ )  $\delta$  (ppm) 7.72 (s, 1H), 7.61 (d,  $J = 7.9$  Hz, 1H), 7.51 (d,  $J = 7.8$  Hz, 1H), 1.21–1.15 (m, 63H).

$^{13}\text{C}$  NMR (126 MHz,  $\text{CDCl}_3$ )  $\delta$  (ppm) 184.8, 183.6, 151.1, 151.0, 144.2, 137.2, 136.1, 134.3, 114.9, 114.8, 114.7, 113.6, 113.1, 111.4, 106.9, 102.1, 102.0, 101.5, 100.6, 94.8, 18.8, 18.77, 18.75, 11.5, 11.26, 11.24. HR-ESI-MS  $m/z$  (%): calcd for  $\text{C}_{47}\text{H}_{71}\text{N}_2\text{O}_2\text{Si}_3^+$  ( $[\text{M} + \text{H}]^+$ ), 779.4823; found 779.4845. UV-vis ( $\text{CHCl}_3$ ):  $\lambda_{\text{max}}$  ( $\epsilon$ ) = 271(61 145), 319(12 611), 533 nm ( $15\ 000\ \text{M}^{-1}\ \text{cm}^{-1}$ ).

**4.2.4. 4-TIPS-DAAQ.** Deep purple solid (498 mg, 10%).  $^1\text{H}$  NMR (400 MHz,  $\text{CDCl}_3$ )  $\delta$  (ppm) 7.70 (s, 2H, H-C(3)), 1.20–1.16 (m, 84H, H-C(13), H-C(14), H-C(17), H-C(18)).  $^{13}\text{C}$  NMR (101 MHz,  $\text{CDCl}_3$ )  $\delta$  (ppm) 183.7 (C9), 150.7 (C1), 143.9 (C3), 135.5 (C4a), 114.6 (C2), 113.7 (C4), 110.8 (C10a), 106.7 (C15), 102.0 (C16), 100.8 (C11), 94.6 (C12), 18.8 (C18), 18.7 (C14), 11.6 (C17), 11.2 (C13). HR-ESI-MS  $m/z$  (%): calcd for  $\text{C}_{58}\text{H}_{91}\text{N}_2\text{O}_2\text{Si}_4$  ( $[\text{M} + \text{H}]^+$ ), 959.6158; found 959.6198. UV-vis ( $\text{CHCl}_3$ ):  $\lambda_{\text{max}}$  ( $\epsilon$ ) = 272(61 294), 318(15 708), 542 nm ( $14\ 816\ \text{M}^{-1}\ \text{cm}^{-1}$ ).

**4.3. Synthesis of 1,5-Diamino-2,6-diethynylanthracene-9,10-dione (2).** To a solution of **2-TIPS-DAAQ** (500 mg, 0.84 mmol) in 20 mL of THF, kept under argon in a single-neck RB flask was added the tetra-*n*-butylammonium fluoride (TBAF) solution (1 M in THF, 1.67 mL) dropwise at 0 °C. Then, the reaction mixture was stirred at room temperature for an additional 2 h. Then, THF was evaporated off in a rotavapor, and the resulting semisolid crude was directly subjected to silica gel column chromatography using methanol/DCM (1:9) to obtain a brick-red solid **2** (217 mg, 91%).  $^1\text{H}$  NMR (500 MHz,  $\text{CDCl}_3$ )  $\delta$  (ppm) 7.67 (d,  $J = 7.8$  Hz, 2H), 7.57 (d,  $J = 7.8$  Hz, 2H), 3.65 (s, 1H).  $^{13}\text{C}$  NMR (126 MHz,  $\text{CDCl}_3$ )  $\delta$  (ppm) 184.3, 151.9, 137.8, 135.6, 114.5, 113.6, 113.0, 87.5, 78.8. HR-ESI-MS  $m/z$  (%): calcd for  $\text{C}_{18}\text{H}_{11}\text{N}_2\text{O}_2$  ( $[\text{M} + \text{H}]^+$ ), 287.0821; found 287.0811. UV-vis ( $\text{CHCl}_3$ ):  $\lambda_{\text{max}}$  ( $\epsilon$ ) = 243(42 507), 496 nm ( $14\ 981\ \text{M}^{-1}\ \text{cm}^{-1}$ ).

**4.4. Synthesis of 2-Ph-DAAQ.** To a two-necked RB flask kept under a positive Ar flow were added **2** (200 mg, 0.70 mmol), iodobenzene (356 mg, 1.75 mmol), Pd( $\text{PPh}_3$ )<sub>2</sub>Cl<sub>2</sub> (24 mg, 0.03 mmol), and CuI (13 mg, 0.06 mmol). THF (10 mL) and triethylamine (10 mL) were purged with Ar for 10 min and then added to the previously mixed reagents, and the reaction mixture was stirred for 2 h at 40 °C until complete consumption of **2** was observed by TLC. The solvent was evaporated, and the reaction mixture was directly loaded on a silica gel column and eluted with methanol/DCM (1:49) to afford **2-Ph-DAAQ** as a dark-purple solid (251 mg, 82%).  $^1\text{H}$  NMR (500 MHz,  $\text{CDCl}_3$ )  $\delta$  (ppm) 7.71 (d,  $J = 7.8$  Hz, 2H), 7.63 (d,  $J = 7.8$  Hz, 2H), 7.60–7.56 (m, 4H), 7.42–7.38 (m, 6H).  $^{13}\text{C}$  NMR (126 MHz,  $\text{CDCl}_3$ )  $\delta$  (ppm) 185.0, 151.0, 137.3, 135.1, 131.7, 129.1, 128.6, 122.3, 115.7, 114.9, 113.4, 99.1, 84.4. HR-ESI-MS  $m/z$  (%): calcd for  $\text{C}_{30}\text{H}_{19}\text{N}_2\text{O}_2$  ( $[\text{M} + \text{H}]^+$ ), 439.1447; found 439.1464. UV-vis ( $\text{CHCl}_3$ ):  $\lambda_{\text{max}}$  ( $\epsilon$ ) = 282(58 262), 319(15 277), 523 nm ( $26\ 011\ \text{M}^{-1}\ \text{cm}^{-1}$ ).

## ■ ASSOCIATED CONTENT

### Supporting Information

The Supporting Information is available free of charge at <https://pubs.acs.org/doi/10.1021/acsomega.2c03609>.

Spectral data and computational details (PDF)

Cartesian coordinates for optimization (TXT)

## AUTHOR INFORMATION

### Corresponding Author

Anjan Bedi – Department of Chemistry, SRM Institute of Science and Technology, Chennai 603203, India;  
orcid.org/0000-0001-6418-4409;  
Phone: +918509216129; Email: anjanb@srmist.edu.in

### Authors

Ganesh Masilamani – Department of Chemistry, SRM Institute of Science and Technology, Chennai 603203, India  
Harikrishna Batchu – Institute of Chemistry, The Hebrew University of Jerusalem, Jerusalem 91904, Israel  
Dana Amsallem – Institute of Chemistry, The Hebrew University of Jerusalem, Jerusalem 91904, Israel

Complete contact information is available at:  
<https://pubs.acs.org/10.1021/acsomega.2c03609>

### Author Contributions

◆ G.M. and H.B. contributed equally to the experimental work. All authors have given approval to the final version of the manuscript. D.A. characterized cyclic voltammetry. A.B. designed, planned, and supervised the project.

### Notes

The authors declare no competing financial interest.

## ACKNOWLEDGMENTS

The authors gratefully acknowledge financial support from SERB, India (SERB/SRG/2021/000648) for funding this research. The authors acknowledge Prof. Ori Gidron, the Hebrew University of Jerusalem, Israel for providing some characterization facilities and fruitful discussions. The authors thank Dr. G. Rama Krishna, CSIR-NCL, Pune for useful discussion. High Performance Computing Centre, SRM Institute of Science and Technology is acknowledged for providing the computational facility.

## REFERENCES

- (1) Zollinger, H. Color Chemistry. Synthesis, Properties and Applications of Organic Dyes and Pigments. *Angew. Chem., Int. Ed.* **2004**, *43*, 5291–5292.
- (2) Salabert, J.; Sebastián, R. M.; Vallribera, A. Anthraquinone Dyes For Superhydrophobic Cotton. *Chem. Commun.* **2015**, *51*, 14251–14254.
- (3) Sims, M. T.; Abbott, L. C.; Cowling, S. J.; Goodby, J. W.; Moore, J. N. Molecular Design Parameters of Anthraquinone Dyes for Guest–Host Liquid-Crystal Applications: Experimental and Computational Studies of Spectroscopy, Structure, and Stability. *J. Phys. Chem. C* **2016**, *120*, 11151–11162.
- (4) Sreenath, M. C.; Joe, I. H.; Rastogi, V. K. Third-Order Optical Nonlinearities of 1,5-Diaminoanthraquinone for Optical Limiting Application. *Opt. Laser Technol.* **2018**, *108*, 218–234.
- (5) Geysens, P.; Evers, J.; Dehaen, W.; Franssaer, J.; Binnemans, K. Enhancing the Solubility of 1,4-Diaminoanthraquinones in Electrolytes for Organic Redox Flow Batteries through Molecular Modification. *RSC Adv.* **2020**, *10*, 39601–39610.
- (6) Zhang, G.; Li, L.; Chen, M.; Yang, F. Chitosan Cross-linked Poly(aminoanthraquinone)/Prussian Blue Ternary Nitrogen Precursor-Derived Fe–N–C Oxygen Reduction Catalysts for Microbial Fuel Cells and Zinc–Air Batteries. *J. Mater. Chem. A* **2020**, *8*, 9256–9267.
- (7) Winter, T.; Bitsch, M.; Müller, F.; Voskian, S.; Hatton, T. A.; Jacobs, K.; Presser, V.; Gallei, M. Redox-Responsive 2-Aminoanthraquinone Core–Shell Particles for Structural Colors and Carbon Capture. *ACS Appl. Polym. Mater.* **2021**, *3*, 4651–4660.
- (8) Zheng, J. Y.; Yan, Y.; Wang, X.; Zhao, Y. S.; Huang, J.; Yao, J. Wire-on-Wire Growth of Fluorescent Organic Heterojunctions. *J. Am. Chem. Soc.* **2012**, *134*, 2880–2883.
- (9) Takeda, T.; Kasahara, Y.; Akutagawa, T. Color-Tunable Arylaminoanthraquinone Dyes through Hydrogen-Bond-Assisted Charge Transfer Interaction. *RSC Adv.* **2021**, *11*, 24217–24231.
- (10) Dahiya, P.; Choudhury, S. D.; Maity, D. K.; Mukherjee, T.; Pal, H. Solvent Polarity Induced Structural Changes in 2,6-Diamino-9,10-Anthraquinone Dye. *Spectrochim. Acta, Part A* **2008**, *69*, 134–141.
- (11) Bedi, A.; Armon, A. M.; Diskin-Posner, Y.; Bogoslavsky, B.; Gidron, O. Controlling the Helicity of  $\pi$ -Conjugated Oligomers by Tuning the Aromatic Backbone Twist. *Nat. Commun.* **2022**, *13*, No. 451.
- (12) Addition of 6 equiv of bromine to 1,5-DAAQ and Sonogashira coupling of the products using 12.5 equiv of TIPS-acetylene could not result in penta or hexa-TIPS substituted DAAQs. This may be due to either an electronic (four –Br atoms deactivates the ring) or a steric factor.
- (13) Sims, M. T.; Mandle, R. J.; Goodby, J. W.; Moore, J. N. Guest–Host Systems Containing Anthraquinone Dyes with Multiple Visible Transitions Giving Positive and Negative Dichroic Order Parameters: An Assessment of Principal Molecular Axes and Computational Methods. *Liq. Cryst.* **2017**, *44*, 2029–2045.
- (14) Rajasingh, P.; Cohen, R.; Shirman, E.; Shimon, L. J. W.; Rybtchinski, B. Selective Bromination of Perylene Diimides under Mild Conditions. *J. Org. Chem.* **2007**, *72*, 5973–5979.
- (15) Suganthi, G.; Meenakshi, C.; Ramakrishnan, V. Preferential Solvation Studies of 1, 5-Diaminoanthraquinone in Binary Liquid Mixtures. *J. Fluoresc.* **2010**, *20*, 95–103.
- (16) Yan, C.; Barlow, S.; Wang, Z.; Yan, H.; Jen, A. K.-Y.; Marder, S. R.; Zhan, X. Non-Fullerene Acceptors for Organic Solar Cells. *Nat. Rev. Mater.* **2018**, *3*, 18003–18021.
- (17) Seidel, N.; Seichter, W.; Weber, E. 1,5-Diamino-2,6-Dibromo-9,10-Anthraquinone. *Acta Crystallogr., Sect. E* **2012**, *68*, o838.